Title: On the reproductive mechanism of Gram-negative protocells

Dheeraj Kanaparthi[1&2*], Marko Lampe[4], Baoli Zhu[2&4], Andreas Klingl[5], Tillmann Lueders[2*] & Petra Schwille[1*]

Affiliations:

[1]Max-Planck Institute for Biochemistry, Munich, Germany.

[2]Chair of Ecological Microbiology, BayCeer, University of Bayreuth, Germany.

[3]Advanced Light Microscopy Facility, European Molecular Biology Laboratory, Heidelberg, Germany.

[4]Key Laboratory of Agro-ecological Processes in Subtropical Regions, CAS, Changsha, China.

[5]Department of Biology, LMU, Planegg-Martinsried, Germany.

Abstract: One of the major challenges of understanding early life or a bottom-up approach of building a synthetic cell is to drive the process of reproduction. To achieve reproduction completely independent of molecular biological processes, here we worked with bacterial protoplasts under environmental conditions of early Earth. Rather than reproducing in a chaotic manner due to the loss of molecular biological co-ordination, cells in our study reproduced in a defined sequence of steps. Lifecycle of cells in our study was either similar to lipid vesicles undergoing osmotic shrinkage or to lipid vesicles undergoing expansion when placed in an elongational flow path. Fission of parent cell into multiple daughter cells was achieved via forces intrinsic to cell like the Brownian motion of intracellular constituents, asymmetric conditions on either side of the membrane or induced by membrane phase-

separation. In short, our study demonstrates how cells reproduced prior to the evolution of molecular biological processes.

Key words:

Introduction: Life on Earth is thought to have emerged in a series of steps described by the theory of chemical evolution[1]. According to this theory organic compounds required for building a cell were synthesized by Miller-Urey[2] like processes and subsequent prebiotic chemical reactions[3–5]. Eventually these organic compounds coalesced to form a protocell[6,7]. These protocells were thought to have been very primitive and can essentially be described as lipid vesicles with internal chemical reactions. Unlike the present-day cells, whose morphology, growth, and reproductive processes are tightly controlled by molecular biological processes, such processes in protocells are thought to have been determined by physical and chemical properties of its constituents[7,8]. Despite being a key evolutionary link between prebiotic chemical reactions and prokaryotes, protocells to date remained a theoretical possibility with no definitive proof for their existence on early Earth, nor was it demonstrated that physical and chemical properties of cell constituents alone could mediate complex biological processes like cell replication. In the present study we attempted to achieve cell fission leading to formation of metabolically viable daughter cells, mediated entirely by physicochemical properties of cell constituents.

Our study differs from earlier studies on protocells in two key aspects. First, rather than the conventional choice of using lipid vesicles, here we used protoplasts of the Gram-negative bacterium *Rhodobacter sphaeroides* (*RS-P*) as a proxy protocell. In our opinion, bacterial protoplasts better simulate a primitive protocell than lipid vesicles for several reasons.

Protoplasts are physiologically and chemically more complex than lipid vesicles. Most likely, even the most primitive self-replicating protocells should have been more complex in their chemical composition than typical lipid vesicles. Despite possessing an internal metabolism, protoplasts like the protocells, lack the innate ability to regulate either their morphology or reproduction[9,10]. As a second novelty of our study, we grew these protoplasts under environmental conditions of early Earth. We believe growing protoplasts under these conditions is necessary as cells reproducing by these processes could only have been native to early Earth. Moreover, given the fact that environmental conditions are known to determine physicochemical properties of cell constituents[11], we think it would be crucial to do these experiments under the environmental conditions of early Earth.

The exact environmental conditions of early Earth is a matter of debate among researchers; nevertheless, recent consensus among researchers suggests that surface temperatures of Archaean Earth (4000-2500 million years ago) ranged between 26° to 35°C[12,13] and Archaean Eon ocean were 1.5 to 2 times saltier than the current oceans[14]. To replicate these conditions, we grew *RS-P* in half strength nutrient broth (NB) supplemented with 5-10% Dead Sea salt (DSS) at 30°C. DSS was used in our incubations rather than pure NaCl to replicate complex salt composition of Archaean oceans[15,16]. Ones we obtained stable protoplasts (*RS-P*), we transferred them into fresh growth media and monitored their morphological transformation at regular intervals. In the below sections of the manuscript, we present an in-depth morphological transformation of *RS-P*, together with an explanation of the physicochemical mechanisms driving such transformations.

Results and Discussion:

Morphological transformation of *RS-P* was monitored at regular intervals by staining and observing the cells using a wide array of Super-resolution microscopic techniques. A simplistic version of *RS-P*'s lifecycle is presented in Figure 1.

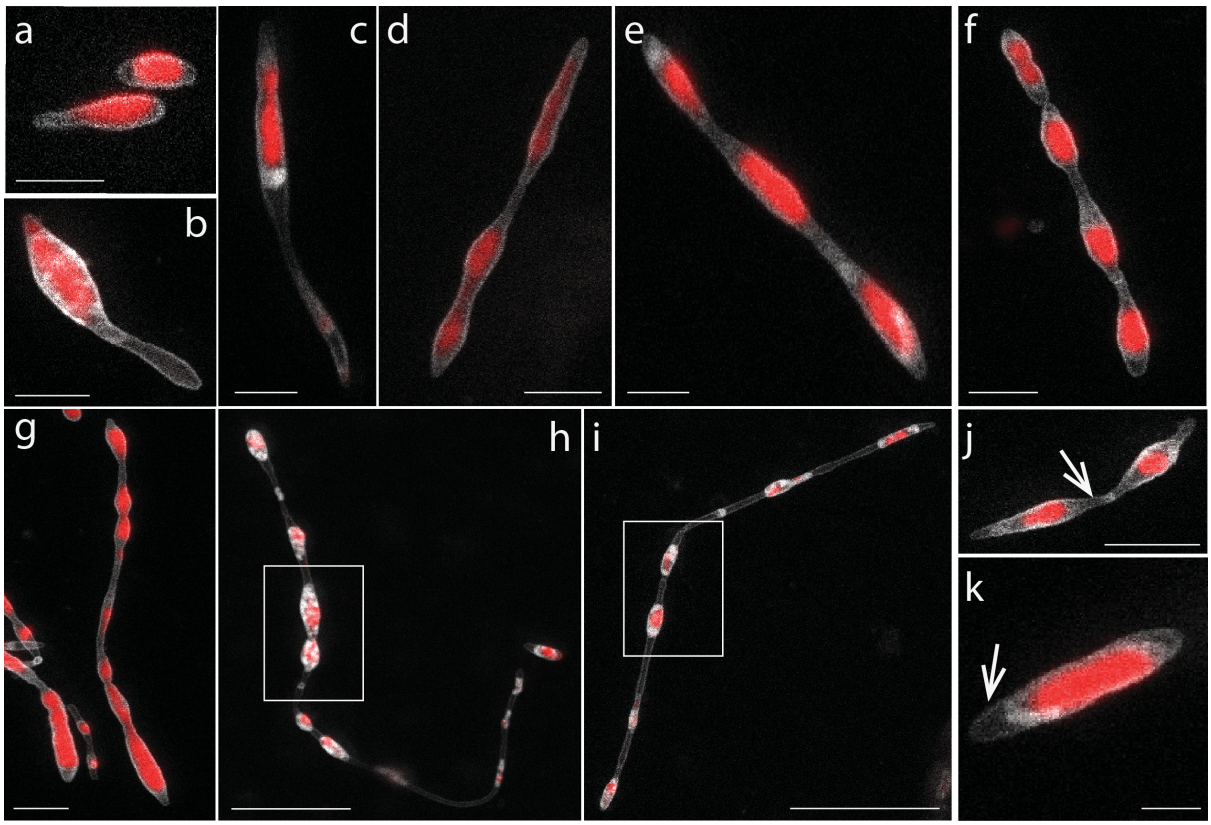

Figure 1. STED microscope Images of *RS-P's* lifecycle (a-k). Cells in these images were stained with universal membrane stain, FM™5-95 (white) and DNA stain, PicoGreen™ (red). Boxes in images h & i show cytoplasmic compartments within the cell undergoing binary fission. Images h-k shows fragmentation of filaments into individual daughter cells. Arrows in these images' points to left-over membrane after cell fission. Scale bars: 1µm (a-g, i & j) and 10µm (h & i).

During the lag phase, growth was restricted to the outer membrane of the cell, which expanded to form a hollow filamentous extension (Figure 1b, c & S1). The length of this tail varied from cell-to-cell, ranging between 0.5 to 5 µm (Figure 1b, 1c & Figure S1a). Based on

our observations we propose a two-step process by which the hollow membrane extensions were formed. In the first step, disproportionately high lipid synthesis in comparison to cytoplasmic volume increase in *RS-P* (low growth rate during lag-phase) should have facilitated transformation of excess membrane into a bud (Figure S1e). This phenomenon of excessive lipid synthesis in bacterial protoplasts was reported by earlier studies[17]. Subsequently these hollow buds dethatched from the inner membrane and were released into the space between outer and inner membranes (periplasmic space). Transmission electron microscope (TEM) images of this growth stage *RS-P*, show the presence of such buds in the periplasmic space (Figure S1e). In step two, these hollow vesicles fused and incorporated into the outer membrane, leading its expansion and formation of hollow filamentous structure (Figure 1b & Figure S1 e-g).

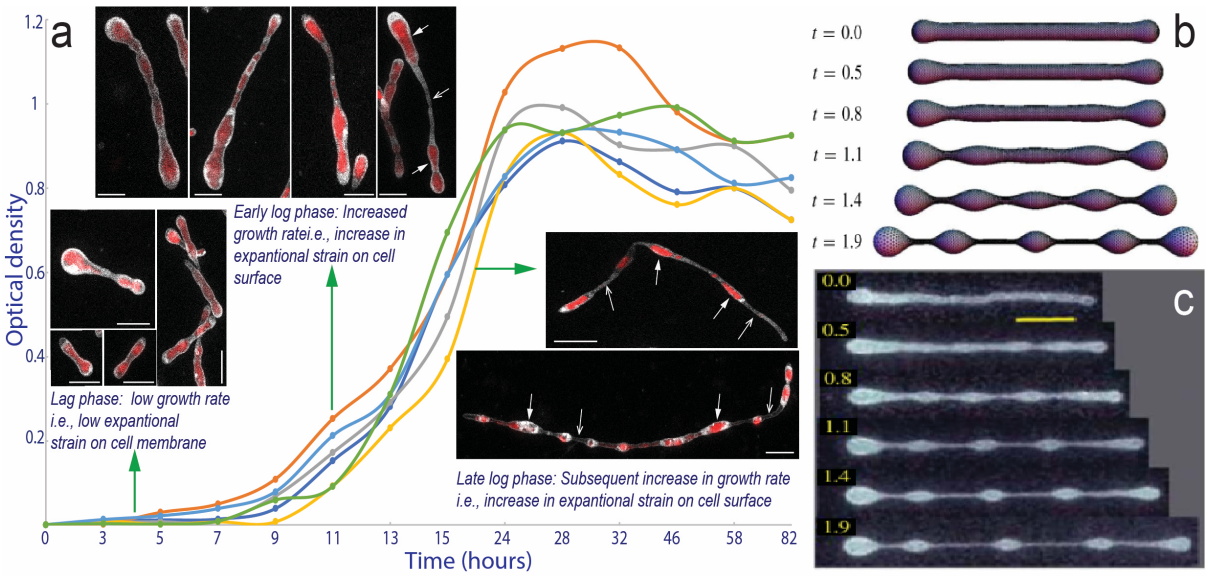

Figure 2. Image a show growth curve and morphologies of *RS-P* in different growth stages. Closed and open arrows in the image points to regions of the cell with cytoplasm and hollow outer membrane connecting the cytoplasmic compartments respectively (also shown in Figure 4 & S2). Images b & c show theoretically predicted, and experimentally observed

morphologies of vesicles subjected to elongational stress over time (t) (originally published by Narsimhan et al., 2015[18] and Kantsler et al., 2008[19]). Scale bar: 1μm (lag & early log-phase), 10μm (late log-phase).

During the early-log phase, with an increase in the growth rate, volume of the cytoplasm increased, gradually filling in the hollow template created by the outer membrane (Figure 1c, d & Figure S1a, b, e & g). This led to transformation of cells in sequence from spherical to tubular cells (Figure 2a) and then into filamentous cells with cytoplasm mostly restricted to either ends of the cell, resembling dumbbells with long filamentous connections (Figure 2, early log-phase).

In the subsequent growth stages, cells developed surface depressions along their length resembling tubular vesicles subjected to curvature-induced destabilization at their surface (like Rayleigh-Plateau instability) (Figure 1d-g & 2-late log phase). These surface depressions were formed as a result of cytoplasmic compartment surrounded by inner membrane undergoing binary fission (Figure 1 d-h). In some filamentous cells we observed cytoplasmic compartments undergoing a symmetric division leading to the formation of daughter cells of equal sizes (Figure 1e & f). In such cells, surface depressions are uniform in size and regularly spaced. Alternately, some cells developed unevenly sized depressions with a large lenticular structure either at the tip (Figure 3, S1b-d & S3) or center of the filament (Figure 3 & S3). Such structures were formed due to asymmetric division of cytoplasmic compartments. Over time these surface depressions grew in depth and two adjacent cytoplasmic compartments were linked to each other only by a hollow strand of outer membrane (boxed regions in Figure 1h, 1i & Figure 2 – late log phase). Rupture of these outer membrane links led to the formation of individual daughter cells (Figure 1h-k).

Transformation of cells from spherical into string of beads morphology, in this exact sequence was reported earlier in lipid vesicles (LVs) undergoing expansion in a laminar flow path[9,20] and in LVs undergoing osmotic shrinkage[20,21]. The above presented morphological transformation of *RS-P* can be explained by similar physiochemical mechanisms.

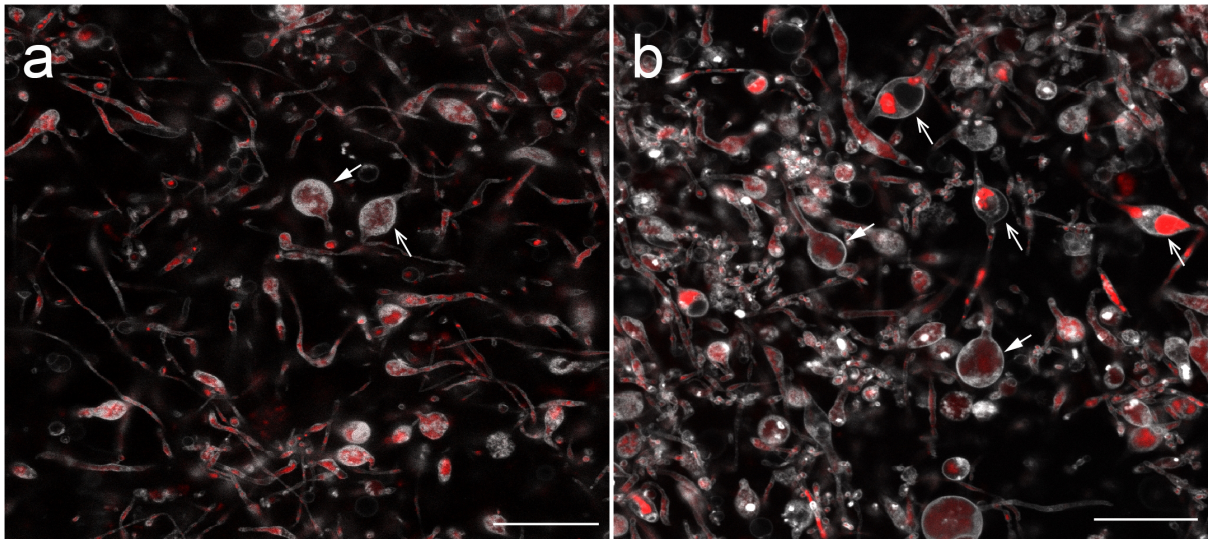

Figure 3. Images a & b show *RS-P* cells in their stationary growth stage. Cells were stained, imaged and color coded as described in Figure. 1. Images show lenticular structures within (open arrows) or at one end (closed arrows) of the filamentous cells. Most lenticular cells contain intracellular membrane vesicles, giving them a reticulate appearance (Figure S3). Scale bars: 10μm.

Growth (or expansion) of cytoplasmic compartment of *RS-P*, gradually filling the void left by outer membrane resembles vesicle undergoing stretching when placed in an elongational flow path (Figure 2 & S4). Morphological transformation of vesicles undergoing such stretching is dependent on expansional strain and elasticity of their membranes[18,19]. Vesicles experiencing a low elongational strain are shown to transformed into prolate or tubular shapes[19] (Figure 2b&c). However, at a certain strain level (threshold strain), vesicles

transformed into a dumbbell morphology. Any further increase in the strain, vesicles formed elongated dumbbells with beaded structures appearing along its length. *RS-P* exhibited a similar pattern of morphological transformation (Figure 2 & S2). In case of *RS-P*, high and low elongational strains on the membrane translate into high and low growth rates. In accordance with our presumption, short prolate or tubular cells were most frequently observed during an early lag-phase, when the growth rate of the cell was slower compared to other stages (Figure 2). With an increase in their growth rate *RS-P* transformed into a dumbbell shape (Figure 2). During the mid-log phase, they formed elongated dumbbells with beaded structures along its length (Figure 2). Subsequent reduction in the growth rate during stationary phase, transformed *RS-P* into string-of-beads morphology (Figure 1h & I, 2 and S2). Continuous transfer of log-phase cells every few hours into fresh media resulted in thicker and longer tubular *RS-P* cells. Unlike the cells in our batch incubations, these cells did not develop surface deformations (Figure S4). These results suggest that rate of cytoplasmic volume increase (growth rate) of *RS-P* played an important role in determining *RS-P*'s morphology.

Along with the growth rate, morphological transformation of *RS-P* can also be explained from a physicochemical perspective. Lifecycle observed in *RS-P* is similar to LVs undergoing osmotic deflation[22]. Sequence of morphological transformations and the end morphology of such vesicles can be explained by Area differential elasticity (ADE) theory[20,21] and is largely determined by the physical properties of the membrane like its elasticity, volume of the cell and the amount of excess membrane. It was experimentally demonstrated that vesicles undergoing osmotic deflation, transform in sequence from spherical to prolate, tubular, then to tubular cells with surface depressions and finally into a string-of-beads morphology to attain a thermodynamically lower energy state[20]. *RS-P*

exhibited a very similar sequence of morphological transformation (Figure 1&2). Like the LVs, excessive lipid synthesis in protoplasts[17] kept *RS-P* in a state of in-equilibrium between surface area of cell membrane and cytoplasmic volume. During the lag-phase, this state of in-equilibrium could have caused *RS-P* to form hollow membrane extensions to accommodate this excess membrane. During the early and mid-log phase, the rate of cytoplasmic volume increase kept pace with membrane synthesis. Hence, cells with membrane overhangs or resembling string-of-beads morphology are largely absent in this growth stage (Figure 2). Gradual decrease in the growth rate by the end of log-phase due to the depletion of nutrients in growth media, caused cells to revert to a state of membrane excess. This high ratio of cell membrane to cytoplasmic volume led to the transformation of cells into a string-of-beads morphology (Figure 1&2). Despite providing a mechanistic explanation for the morphologies of *RS-P*, neither vesicles undergoing LVs undergoing expansion in a laminar flow path[9,20] nor LVs undergoing osmotic shrinkage[20,21], were ever reported to have formed large lenticular cells (Figure 3).

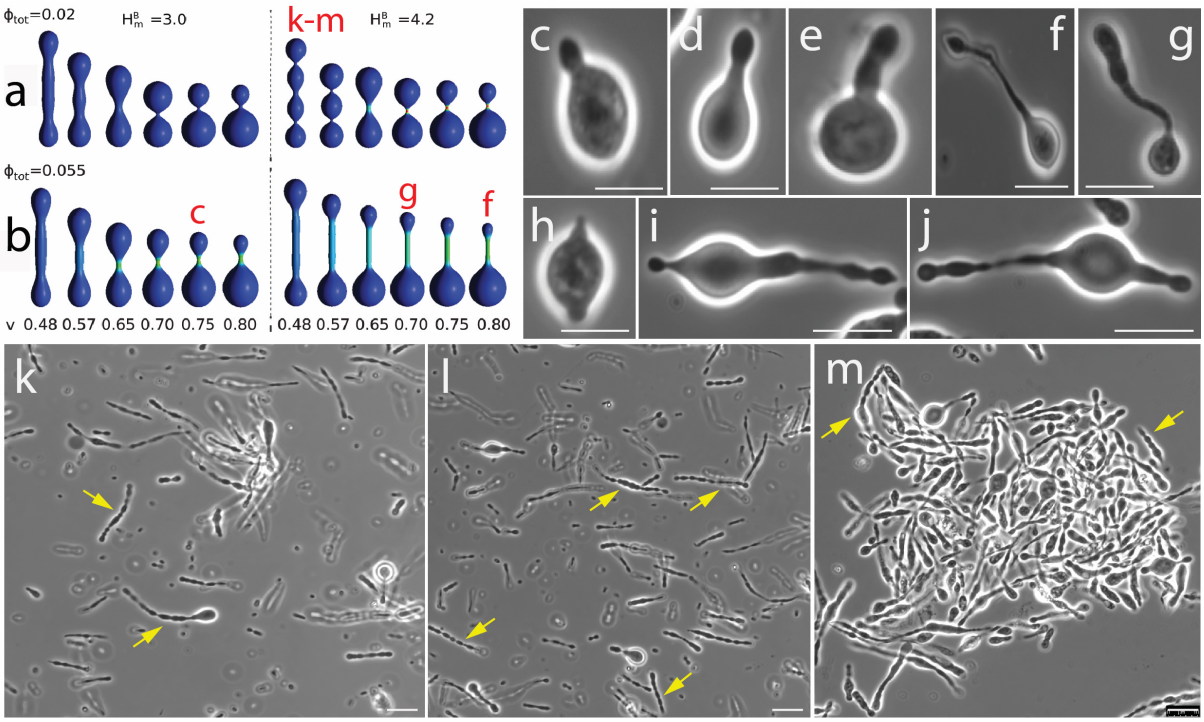

Figure 4. Images a & b show morphologies of vesicles with an anisotropic membrane as predicted from mathematical models[23]. ν-values (X-axis) represent ratio between the actual volume of vesicle to volume of the same vesicle in its spherical form with same surface area, Φ_{tot} – represent the concentration of anisotropic component, H^B_m – represent intrinsic curvature of the anisotropic component (originally published by Bobrovska *et al*., 2013). Images c-g, show lag and early log phase cells, that were very similar to the mathematically predicted morphologies (indicated by letters in red over the predicted shapes in image b). Decrease in the reduced volume (ν) in live cells translates into gradual reduction of lipid: cell volume (from lag to log phase). Images c-j show log-phase cells undergoing asymmetric cell division leading to the formation of large lenticular cells. Images k-m show late-log phase *RS-P* cells, beginning to transform into a string-of-beads morphology (arrows). Scale bars: 2μm (c-j) and 10μm (k-m).

Formation of large lenticular or spheroid structures (Figure 3) with filamentous extensions could be explained by anisotropy in physical properties of cell membrane[23] (Figure 4). Biophysical studies focused on understanding morphology and cell replication are mostly a result of studying vesicles of rather simpler lipid composition. In such studies, it is generally assumed that the physical properties of vesicle membrane like fluidity and elasticity are isotropic throughout their surface. Unlike LVs, cell membranes have a complex lipid composition and are intercalated with proteins. This leads to lateral heterogeneity or anisotropy in their physical properties[24]. It was hypothesized that such differences could result in an un-uniform expansion and deformation of membrane surface during osmotic deflation, leading to an asymmetric cell division and possibly to the formation of lenticular structures[23] (Figure 4a & 4b). Like shown in Figure 4b, formation of thin tubular protrusions

from a spherical cell is thermodynamically only possible in anisotropic membranes. Morphological transformation we observed in *RS-P* is very similar to the theoretical predictions on the behavior of vesicles with anisotropic membranes (Figure 4c-m). High rate of cytoplasmic volume increase during the early (log-)growth stages represents a cell state with higher value of ν (reduced volume i.e., the ratio of actual vesicle volume and volume of the volume of the vesicle in spherical form) and high Φ_{tot} (inherently high lateral heterogenicity in live cells) *i.e.,* a state of little to no excess membrane. As predicted by the mathematical models, cells in this growth-stage underwent an asymmetric division (annotations c & d in Figure 4b & 4c & d). Figure S1f&g, show TEM images of *RS-P* cells forming such extensions. Such asymmetric division of cytoplasmic content is predicted to have led to the formation of one tiny spherical and a large lenticular cells[23]. A gradual reduction in the growth rate towards the end of the log-phase could have resulted in lower ν-values in *RS-P*. This reduction together with an increase in the spontaneous curvature of the membrane either due to membrane components or due to excess membrane, could have transforming *RS-P* into a string-of-beads morphology.

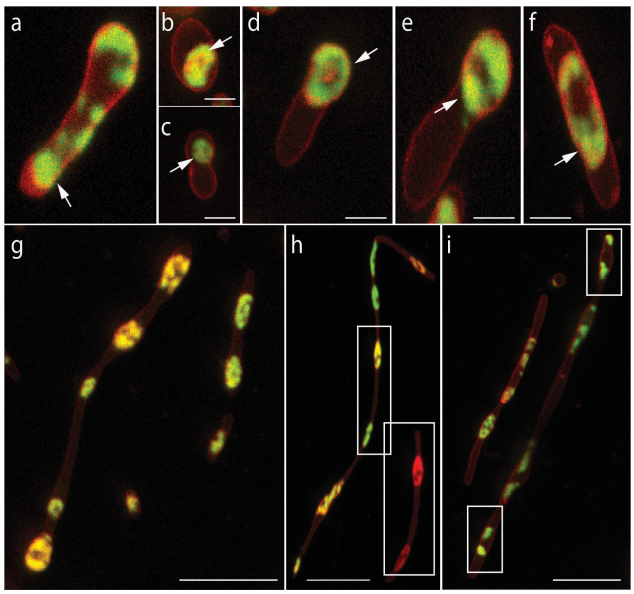

Figure 5. Images a-i show *RS-P* cells of different growth stages. Cells in these images were stained with universal membrane stain, FM™5-95 (red) and membrane stain that specifically stains L_d-membrane, *FAST*™ Dil (green). Closed arrows in images point to regions of the cell with L_d-membrane. Open arrow in image-f, points to vesicle in the periplasmic space of the cell, exclusively composed of L_o-membrane. Insert in image-h show the region of the filament stained only with universal membrane stain. Boxed regions in image-i show cytoplasmic compartments enclosed by inner cell membrane. L_d-membrane within these compartments is localized at the poles. Scale bars: 1μm (a-f) and 10μm (g-i).

Also, in accordance with ADE theory[21], morphological transformation of *RS-P* is associated with membrane phase-separation (Figure 5). The sequential steps of membrane phase-separation observed in *RS-P* is similar to what was proposed by lipid-raft hypothesis[24]. During early growth stages, cell membrane underwent phase-separation with liquid-disordered (L_d) regions forming small patches within the cell membrane (Figure 5a). Overtime inner membrane of the cell is exclusively composed of L_d and outer membrane of the cell is exclusively composed of liquid-ordered (L_o)-membrane (Figure 5b-d). This enrichment of L_d-membrane around the cytoplasm, could have been due to constant loss of L_o-membrane in the form of hollow membrane buds into the periplasmic space (Figure S1). This budding of phase-separated membranes could be explained by the hypothesis proposed by Lipowsky & Jülicher[25,26]. In cells of subsequent growth stages and in cells undergoing binary fission, presence of L_d-membrane was restricted to the poles (Figure 4e & 4f), where membrane experiences a high spontaneous curvature and central barrel connecting the poles was noticed to be composed of L_o-membrane (Figure 5e & 5f). Given the L_d and L_o-membranes are largely composed of unsaturated and saturated phospholipids respectively, we

presume lipid molecules in the membrane underwent self-organization with unsaturated phospholipid rich L_d-membrane translocating to regions of the cells with high spontaneous curvature (the cell poles) and distribution of L_o-membrane being restricted to linear regions of the cell membrane, where membrane experiences a low curvature. Similarly, localization of L_d and L_o-membranes selectively in inner and outer membrane of the cell could also be explained by a combination of physical properties of cytoplasm and organizational principles leading towards a stable and lowest free energy state. Given the constant movement of the cytoplasmic compartment of the cell (Movie S1 & S2), it could have been energetically favorable to encapsulate cytoplasm with more fluid L_d-membrane rather than more rigid L_o-membrane. Lipid raft hypothesis[24] and the existence of phase-separated membrane in live cells has been a point of contention among researchers[27], to date such membrane phase-separation and its physiological significance has only been reported in LVs[28]. To the best of our knowledge, ours is the first study to provide visual evidence of distinct phases in cell membrane (Figure 5) and describe its evolutionary significance.

Earlier studies proposed that fission of a protocells into daughter cells should have been achieved through physical forces[7,29]. Hence to achieve protocell fission, these studies employed methods like extrusion through a narrow pore size filter or by application of external force [7,29,30]. As most of the cells in the last growth stage are primarily unicellular daughter cells that were formed by fission of filamentous *RS-P* and given the fact that our experiments were conducted under static conditions, we do not assume fission of cells was a result of an external stimulus. We rather propose that fission of daughter cells was achieved by forces internal to the cell and was either a result of internal metabolic reactions[31] or Brownian motion of intracellular constituents[32]. It was also hypothesized that presence of internal metabolism could lead to shape instabilities on the cell surface ultimately leading to

cell division[31]. Morphologies and reproductive processes similar to the ones observed in *RS-P* were recently reported among lipid vesicles encapsulating vibrating nanoparticles, to simulate Brownian motion of proteins within a cell[32]. Uncanny resemblance between morphologies and reproductive processes of *RS-P* and LVs encapsulating nanoparticles from above mentioned study[32], suggests that reproductive processes could have been determined by the physical forces exerted by intracellular constituents. In support of this presumption, filamentous cells were intrinsically unstable. A constant pull-push motion of individual cells within the filament was often observed in *RS-P* (Movie S3-S5). This constant movement should have been caused by Brownian movement of intracellular constituents (Movie S1 & movement of DNA in spherical *RS-P* cells in the top half of the Movie S2) This constant movement of intracellular constituents could have led to the generation of force required for the fission of daughter cells.

Another factor that could have contributed to constant oscillations on the cell surface which ultimately led to the fission of cells is the asymmetric conditions on either side of the cell membrane – organic carbon within the cell and inorganic salts outside the cell. Together with the movement of intracellular constituents, such conditions are known to induce constant deformation on the membrane surface[33]. In support of this presumption, addition of bactericidal compounds like sodium azide (0.3%)[34] or formaldehyde[35] did not have any influence on the surface deformations of the cells. These constant surface deformations could only be halted when conditions inside and outside the cells were equilibrated by creating pores within the membrane using detergents like Triton X-100 (0.5%), suggesting that asymmetric conditions on either side of the cell membrane contributed to the deformation of cells and provided the force required to mediate cell fission.

Based on the above inferences we argue that fission of parent cell into daughter cells was mediated by physiochemical forces generated by virtue of processing internal metabolism[31], random movement of cytoplasmic constituents (Movie S2), deformations caused by transient binding of cations to the membrane surface[36] and asymmetric environmental conditions on either side of the cell membrane in terms of osmolarity or nature of the solute[33]. All these conditions are shown to generate shape instabilities, which could have led to fission of cells[31] (Movies S3). Nevertheless, relative contribution of each of these processes to the fission of parent cells is hard to determine in live cells, especially given their metabolic and compositional complexity.

To simulate Archaean Eon Ocean salinities, we grew *RS-P* in 5-10% DSS-NB in all the above experiments. DSS is a mixture of several mono and divalent salts like NaCl (38%wt), KCl (9%wt), $MgCl_2$ (42%wt) and other inorganic salts. These cations are known to interact differently with phospholipid membranes and are known to alter their physical properties[11,33]. Hence, in the subsequent experiments we attempted to understand the influence of individual salts on the morphology of *RS-P*. To test this, we repeated the above experiments replacing DSS with equivalent concentration of divalent and monovalent salts like $MgCl_2$ or KCl/NaCl. When grown in the presence of monovalent salts (7%KCl-NB), *RS-P* exhibited morphologies and reproduced by processes very similar to the ones observed when grown with DSS (Figure S4); except for forming thicker and longer filamentous cells with larger lenticular structures.

Similar cell morphologies were also observed when *RS-P* was grown in $MgCl_2$, with the exception that cell sizes were considerably smaller (Figure S5). Most cells observed in these incubations were of thin filamentous morphology. Thick tubular cells or lenticular cells with diameter >1-2μm's were rarely observed (sometimes only transiently during the mid-growth

stages) (Figure S5c, d & e). Unlike when grown in DSS or KCl, cells in their last growth stage were mostly uniform in their morphology (Figure S5i). Cells of this stage are predominantly unicellular daughter cells or cells in dyad undergoing binary fission.

Different morphologies exhibited by *RS-P* when grown in the KCl and $MgCl_2$ could be due to the nature of interaction between phospholipid membranes and different cations[11]. It was reported that divalent cations like Mg^{+2} organizes lipids into clusters of 10-15 molecules each[37]. This in turn dehydrates and increases the stiffness of the membrane making its area expansion energetically unfavorable. On the other hand, monovalent cations like K^+ are known to reduce bending rigidity of the membrane, making the membrane more flexible[33]. This phenomenon could explain easy expansion of cell membrane, conducive for formation of larger cells in the presence of KCl and smaller cell sizes in when grown in the presence of $MgCl_2$.

Cells in all the experiments above were grown under static conditions. Given such conditions are rarely encountered in natural environments, we repeated the above experiments under multiaxial elongational flow conditions by growing *RS-P* on an orbital shaker. Under these growth conditions, cells exhibited a more uniform morphology irrespective of the nature of the salt (Figure S6). Little morphological variation was observed during different growth stages. Most cells during lag, log and stationary growth stages were either individual cells or cells in dyad undergoing binary fission. Other cell morphologies were rarely observed. When *RS-P* was transferred between growth media containing different salt compositions or grown under static or stirring conditions, morphologies of *RS-P* changed reversibly. This reversible change suggests that morphology of *RS-P* is determined by environmental conditions rather than the information encoded in its genome.

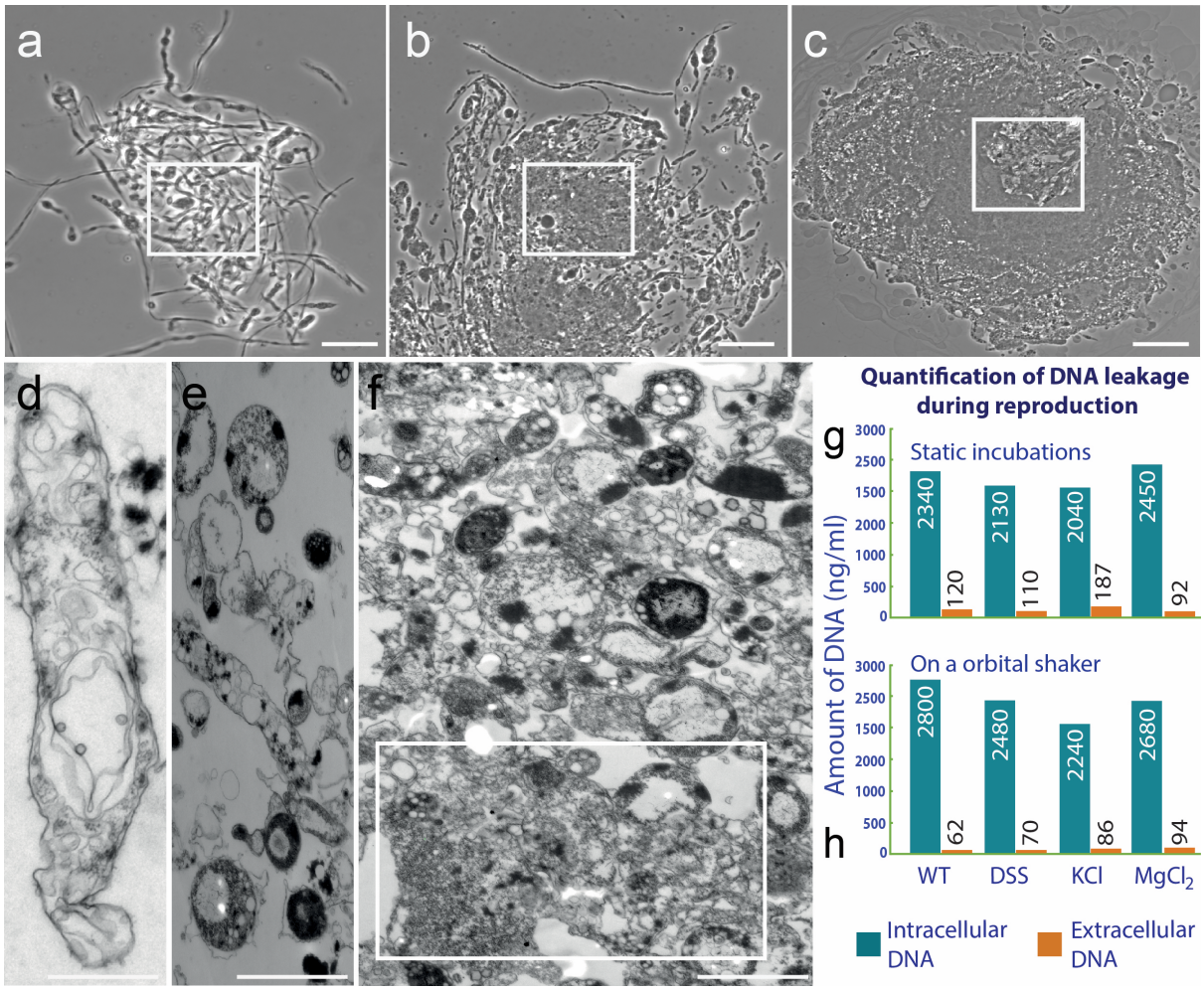

Figure 6. Images a-c are phase-contract images of *RS-P* during different growth stage. The boxed regions show entanglement of filamentous cells leading to formation of debris. Images d-f are TEM images of stationary growth stage cells. This stage consists of cells that were depleted in their cytoplasm and considerable amount of membrane debris (boxed region in c). Images e & f show a comparison of the amount (n=5) of extracellular and intracellular DNA (ng/ml), when *RS-P* was grown under static conditions (g) and while shaking (h). Annotations, WT (wild type, *R. sphaeroides* with a cell wall grown in NB); DSS, KCl & $MgCl_2$ – *RS-P* grown in NB with respective salts. Scale bar: 10µm (a-c) & 1µm (d-f).

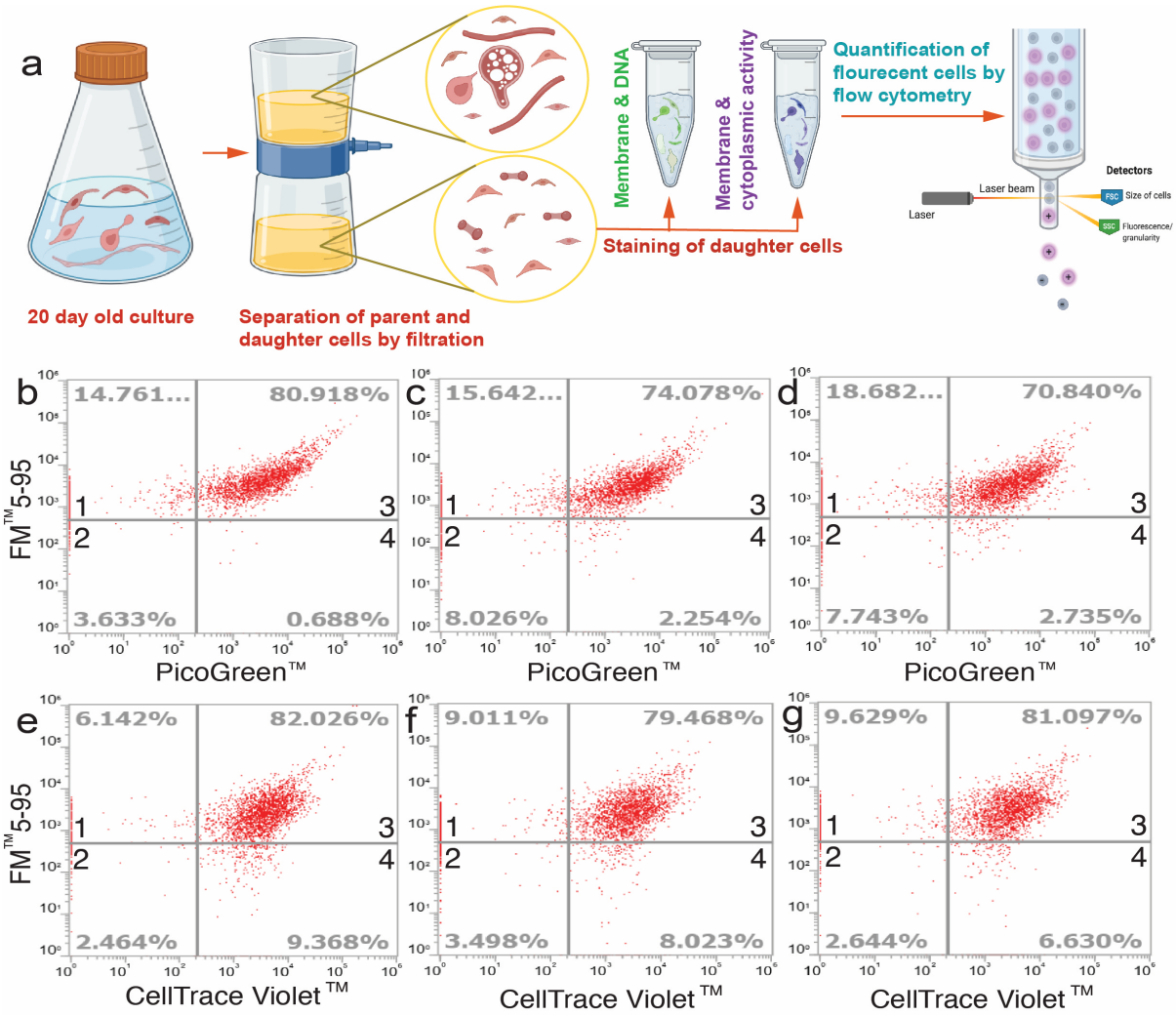

Figure 7. Panel-a show the workflow of the experiment. Images b-d show flowcytometric quantification of cells with an intact membrane and intracellular DNA. Quadrants 1, 2, 3 & 4 in each plot represent the percentage of cells stained with only FM™5-95 (1), cells stained only with PicoGreen™ (2), cells stained by both FM™5-95 & PicoGreen™ (3) and cells that were not stained by either dye (4). Images e-g show flowcytometric quantification of cells with an intact membrane and cytoplasmic activity. Quadrants 1, 2, 3 & 4 in each plot represent the percentage of cells stained with only FM™5-95 (1), cells stained with only CellTrace™ Violet (2), cells stained by both FM™5-95 & CellTrace™ Violet (3) and cells that cells that were not stained by either dye (4).

Reproductive efficiency of *RS-P* is determined by quantifying the leakage of cell constituents during RS-P's lifecycle[7]. Comparison of DNA concentrations within and out of the cell during late log phase (Figure 6g & 6h), suggests that *RS-P* reproduced with a similar efficiency as cell in their native form with functioning molecular biological mechanisms. Given the considerable amount of membrane debris (Figure 6) observed during the stationary growth phase, we propose that *RS-P* reproduced rather inefficiently. Nevertheless, reproductive efficiency was dependent on the environmental conditions (Figure 6). Relatively less wastage of cell constituents and production of membrane debris was observed when *RS-P* was grown in the presence of $MgCl_2$ (Figure S5) than when cultured in DSS or KCl. Reproductive efficiency was also higher when *RS-P* was cultured under non-static conditions (Figure 6). Despite the wastefulness of its reproduction process under some environmental conditions, all our incubations resulted in viable daughter cells with cytoplasmic activity and intracellular DNA (Figure 7). Subsequent transfer of these cells either directly or after passing through 0.44μm filter (Figure 7) to separate daughter cells from other large cells and membrane debris into fresh media always resulted in growth. This mechanism of reproduction and the efficiency of the process is comparable to theoretical propositions of protocell reproduction[7], proposed from studying LVs.

Conclusion: Our work alters the current presumption that molecular biological processes are necessary for mediating complex biological processes like cell-replication. Our observations suggest that reproduction is an innate physicochemical property of cells with internal metabolism. In the absence of molecular biological processes, cell reproduction is governed by physiochemical properties of the cell constituents. Nevertheless, efficiency of the process is considerably lower in cell devoid of molecular biological mechanisms. Given the simplicity and efficiency with which cells reproduced under environmental conditions of

early Earth, we propose that primitive protocells inhabiting early Earth could have reproduced in a similar way. In our subsequent work, we were able to demonstrate from the fossil record that cells reproducing by above described processes in-deed existed on early Earth[38].

Author contributions: DK conceived the work with input from TL, BZ, ML & PS. DK performed laboratory experiments. AK did TEM imaging. DK & ML performed confocal super-resolution light microscopy imaging. DK wrote the manuscript with input from TL, BZ, ML, AK & PS. This research was funded by the European Research Council (ERC), grant agreement 616644 (POLLOX) to TL and DFG-TRR174 to PS.

Acknowledgments: We would like to thank Gabriella Berthal and Markus Oster for excellent technical support. We would also like to thank Advanced Light Microscopy Facility at EMBL, Heidelberg, Ulf Schwartz from Leica Microsystems, colleagues at Ecological microbiology (Bayreuth University) and cellular biophysics laboratory (Max Planck institute for Biochemistry) for their support throughout the work. We thank Jan-Hagen Krohn for critical reading of the manuscript.

References:

(1) Oparin, A. I. *R. Inst. Chem. Rev.* **1969**, *2*, 1-12.

(2) Miller, S. L. **1953**, *117*, 528–529.

(3) Mariani, A.; Russell, D. A.; Javelle, T.; Sutherland, J. D. *J. Am. Chem. Soc.* **2018**, *140*, 8657-8661.

(4) Powner, M. W.; Gerland, B.; Sutherland, J. D. *Nature* **2009**, *459*, 239-242.

(5) Rajamani, S.; Ichida, J. K.; Antal, T.; Treco, D. A.; Leu, K.; Nowak, M. A.; Szostak, J. W.; Chen, I. A. *J. Am. Chem. Soc.* **2010**, *132*, 5880-5885.

(6) Chen, I. A.; Salehi-Ashtiani, K.; Szostak, J. W. *J. Am. Chem. Soc.* **2005**, *127*, 13213–13219.

(7) Zhu, T. F.; Szostak, J. W. *J. Am. Chem. Soc.* **2009**, *131*, 5705-5713.

(8) Budin, I.; Debnath, A.; Szostak, J. W. *J. Am. Chem. Soc.* **2012**, *134*, 20812-20819.

(9) Wu, L. J.; Lee, S.; Park, S.; Eland, L. E.; Wipat, A.; Holden, S.; Errington, J. *Nat. Commun.* **2020**, *11, 4149*. https://doi.org/10.1038/s41467-020-17988-7.

(10) Leaver, M.; Dominguez-Cuevas, P.; Coxhead, J. M.; Daniel, R. A.; Errington, J. *Nature* **2009**, *457*, 849-853.

(11) Tsai, H. H. G.; Lai, W. X.; Lin, H. Da; Lee, J. Bin; Juang, W. F.; Tseng, W. H. *Biochim. Biophys. Acta - Biomembr.* **2012**, 1818, 2742-2755.

(12) Blake, R. E.; Chang, S. J.; Lepland, A. *Nature* **2010**, *464*, 1029–1032.

(13) Catling, D. C.; Zahnle, K. J. *Sci. Adv.* **2020**, *6*, eaax1420.

(14) Knauth, L. P. *Nature* **1998**, *395*, 554.

(15) Moore, E. K.; Jelen, B. I.; Giovannelli, D.; Raanan, H.; Falkowski, P. G. *Nature Geoscience*. 2017, *10*, 629-636.

(16) Johnson, T. E.; Brown, M.; Kaus, B. J. P.; Vantongeren, J. A. *Nat. Geosci.* **2014**, *7*, 47-52.

(17) Mercier, R.; Kawai, Y.; Errington, J. *Cell.* **2013**, *152* (5), 997–1007.

(18) Narsimhan, V.; Spann, A. P.; Shaqfeh, E. S. G. *J. Fluid Mech.* **2015**, *777*, 1–26.

(19) Kantsler, V.; Segre, E.; Steinberg, V. *Phys. Rev. Lett.* **2008**. *101*, 048101- 4.

(20) Yanagisawa, M.; Imai, M.; Taniguchi, T. *Phys. Rev. E - Stat. Nonlinear, Soft Matter Phys.* **2010**, *82*, 051928-1-9.

(21) Yanagisawa, M.; Imai, M.; Taniguchi, T. *Phys. Rev. Lett.* **2008**, *100*, 148102-4.

(22) Sanborn, J.; Oglęcka, K.; Kraut, R. S.; Parikh, A. N. *Faraday Discuss.* **2013**, *161*, 167-176.

(23) Bobrovska, N.; Góźdź, W.; Kralj-Iglič, V.; Iglič, A. *PLoS One* **2013**. *8*, 0073941.

(24) Simons, K.; Ikonen, E. **1997**. *387*, 569-572.

(25) Lipowsky, R. *J. Phys. II* **1992**, *2*, 1825-1840.

(26) Jülicher, F.; Lipowsky, R. *Phys. Rev. Lett.* **1993**, *70*, 2964.

(27) Sezgin, E.; Levental, I.; Mayor, S.; Eggeling, C. *Nature Reviews Molecular Cell Biology* **2017**, *18*, 361-374.

(28) Dreher, Y.; Jahnke, K.; Bobkova, E.; Spatz, J. P.; Göpfrich, K. *Angew. Chemie - Int. Ed.* **2021**, *60* 10661-10669.

(29) Deshpande, S.; Spoelstra, W. K.; Van Doorn, M.; Kerssemakers, J.; Dekker, C. *ACS Nano* **2018**, *12,* 2560–2568.

(30) Hanczyc, M. M.; Fujikawa, S. M.; Szostak, J. W. *Science.* **2003**, *302*, 618–622.

(31) Zwicker, D.; Seyboldt, R.; Weber, C. A.; Hyman, A. A.; Jülicher, F. *Nat. Phys.* **2017**, *13*, 408-413.

(32) Vutukuri, H. R.; Hoore, M.; Abaurrea-Velasco, C.; van Buren, L.; Dutto, A.; Auth, T.; Fedosov, D. A.; Gompper, G.; Vermant, J. *Nature* **2020**, *586*, 52-56.

(33) Karimi, M.; Steinkühler, J.; Roy, D.; Dasgupta, R.; Lipowsky, R.; Dimova, R. *Nano Lett.* **2018**, *18*, 7816-7821.

(34) Levy, S.; Chevion, M. *Environ. Toxicol. Chem.* **2009**, *28*, 1380-1389.

(35) Spahn, C.; Grimm, J. B.; Lavis, L. D.; Lampe, M.; Heilemann, M. *Nano Lett.* **2019**, *19*, 500-505.

(36) Tarun, O. B.; Okur, H. I.; Rangamani, P.; Roke, S. *Commun. Chem.* **2020**, 3, article number 17.

(37) Schultz, Z. D.; Pazos, I. M.; McNeil-Watson, F. K.; Lewis, E. N.; Levin, I. W. *J. Phys.*

Chem. B **2009**. *113*, 9932-9941.

(38) Kanaparthi, D.; Lampe, M.; Zhu, B.; Boesen, T.; Klingl, A.; Schwille, P.; Lueders, T. *bioRxiv* **2021**, 2021.08.16.456462.
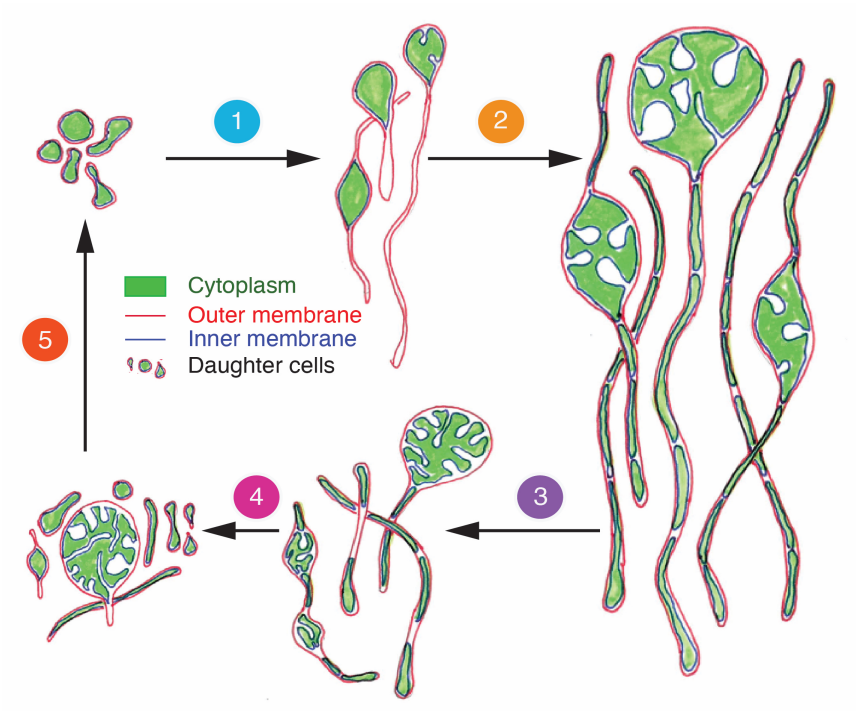
Table of content: Lifecycle of multilamellar protocell